Journal of Physics: Conference Series

PAPER • OPEN ACCESS

Comparison study between wind turbine and power kite wakes

To cite this article: T Haas and J Meyers 2017 *J. Phys.: Conf. Ser.* **854** 012019

Comparison study between wind turbine and power kite wakes

T Haas and J Meyers

Department of Mechanical Engineering, University of Leuven, 3001 Heverlee, Belgium

E-mail: thomas.haas@kuleuven.be, johan.meyers@kuleuven.be

Abstract. Airborne Wind Energy (AWE) is an emerging technology in the field of renewable energy that uses kites to harvest wind energy. However, unlike for conventional wind turbines, the wind environment in AWE systems has not yet been studied in much detail. We propose a simulation framework using Large Eddy Simulation to model the wakes of such kite systems and offer a comparison with turbine-like wakes. In order to model the kite effects on the flow, a lifting line technique is used. We investigate different wake configurations related to the operation modes of wind turbines and airborne systems in drag mode. In the turbine mode, the aerodynamic torque of the blades is directly added to the flow. In the kite drag mode, the aerodynamic torque of the wings is directly balanced by an opposite torque induced by on-board generators; this results in a total torque on the flow that is zero. We present the main differences in wake characteristics, especially flow induction and vorticity fields, for the depicted operation modes both with laminar and turbulent inflows.

1. Introduction

In the past decade, the global cumulative installed wind power capacity has increased significantly. The size of the wind turbines has also been increasing constantly, with modern turbines reaching rotor diameters and hub heights of more than hundreds of meters; this is a logical trend, considering that wind speed increases with height. Already in 1980, Loyd [1] proposed an alternative technology that can tap into high-altitude wind by using tethered aircrafts. Airborne Wind Energy systems present many advantages upon conventional wind turbines. First, at operation altitudes up to 500m, AWE systems can tap into stronger and more consistent winds [2], thus surpassing the capacity factor of conventional wind power [3]. Second, this technology reduces material requirements and third, ground-based electricity generation facilitates the maintenance of such systems[4]. Despite this high potential, this new technology is still in an early development stage and thus not yet competitive with actual conventional wind turbines. Different operation modes are being investigated, among others the so called lift and drag modes[1], but no leading design has yet emerged, and many research efforts go towards insuring reliable operation and autonomous launching and landing.

The present study aims to address the interaction of such airborne wind energy systems with their wind environment. In the context of conventional wind turbines and large clusters of wind turbines, the interaction between the systems and the atmospheric boundary layer has been investigated intensively [5][6][7]. In particular, the wake effects on power generation of downstream turbine rows in wind farms are intensively being studied in current research activities. Thus, an extensive understanding of the wake characteristics is preferable and many studies have been carried out in this field, see [8] and [9] for instance. The complex dynamics of vortical structures accounting for the development of wind turbine wakes have been addressed in [10] and [11]. However in AWE, the interaction between airborne systems and their environment has not yet been thoroughly investigated in this context and thus this paper aims to give first insights on the dynamics of different operation modes.

In his pioneering work [1], Loyd introduced different operation modes for energy harvesting with tethered aircrafts. He first defined the so-called *lift mode*, for which the tethered system pulls a load on the ground while the tether reels out. Power is then generated on the ground via the tension in the tether. Second, he defined the *drag mode* for which additional on-board generators are mounted on the wing, producing electricity that is transferred to the ground via the tether. These small turbines induce additional drag on the wing. A review of the different implemented concepts is given in [12].

Wind turbine blades rotating at a constant angular speed experience a constant torque from the aerodynamic forces. In real systems, this torque is captured by the generator and turned into useful mechanical power. Hence, the blades induce a net torque addition onto the flow, which results in the rotation of the flow in the direction opposite to the blades. In this study, we only consider *blade portions* (approximately the top 30% of the blade length at the tip) that we will refer to as the wings of the system. This wing system rotates at constant angular speed and sweeps an annulus in a vertical plane orthogonal to the main flow direction. The force distribution along the wings span is similar to conventional turbine blades, thus we will refer to this turbine-like operation mode of our wing system as the *turbine mode*. In addition, we will also consider triple-kite systems in drag mode flying in similar configurations. We assume that the additional drag forces are solely acting in the system's rotation plane, in the direction opposite to the tangential component of the aerodynamic lift. The torque of this additional drag balances the aerodynamic torque and thus the resulting torque added to the flow is zero. The aerodynamic force distribution is computed according to the Blade-Element/Momentum theory applied to an optimal, drag-free, blade design [13].

This paper is organized as follows. In section 2, the methodology and the computational framework of the study are introduced. In section 3, numerical results for simulation of both turbine and power modes are presented and discussed. Finally, we conclude this paper with some outlook and motivation for future work in section 4.

2. Simulation framework and methodology

2.1. LES methodology

The simulations are performed using the large-eddy simulation code SP-Wind developed in-house at KU Leuven [6][14][15]. The governing equations are the filtered incompressible Navier-Stokes equations for neutral flows. The continuity and momentum equations are given by

$$\partial_i \tilde{u}_i = 0\,, \tag{1}$$

$$\partial_t \tilde{u}_i + \partial_j \left(\tilde{u}_i \tilde{u}_j\right) = -\partial_i \tilde{p}^* - \partial_j \tau_{ij}^d + f_i \tag{2}$$

where the filtered velocity is denoted by $\tilde{u}_i$, $\tilde{p}^*$ is the filtered modified pressure and τ_{ij}^d is the deviatoric part of the subgrid-scale stress tensor, which is modeled using an eddy-viscosity model. Its trace is included in the filtered modified pressure given by $\tilde{p}^* = \tilde{p}/\rho + \delta_{ij}\tau_{kk}/3$. The effects of the wing system on the flow are modelled using a body force f_i, as discussed further below. The governing equations are discretized using a Fourier pseudo-spectral method in the horizontal directions (x_1, x_2) while in the vertical direction (x_3), a fourth-order energy-conserving finite-difference scheme is used. The horizontal discretization requires periodic boundary conditions which can be circumvented in the streamwise direction x_1 by employing a fringe-region technique [16]. Time integration is performed with a classic four-stage fourth-order Runge Kutta scheme, and the time step is computed using a Courant-Friedrichs-Lewy number of 0.4.

2.2. Force distribution along the wing

The effect of the wing system on the flow is added to the momentum equations via the forcing term f_i. Using an actuator-line technique, as described in [8], we discretize the wings into a finite number of elements for which the aerodynamic forces are computed and subsequently filtered onto the LES grid using a Gaussian convolution filter.

The local force contributions are computed according to the optimality condition given by the Betz-Joukowsky limit [13]. The aerodynamic drag is neglected and so only the lift force on the wing is considered. The lift distribution can be derived from the axial and tangential induction factors, defined as $a = 1/3$ and $a' = a(1-a)/(\lambda^2\mu^2)$ respectively, where λ is the tip-speed ratio and $\mu = r/R$ the normalized radial distance from the virtual rotation center. The lift force L per unit span and the local flow angle ϕ are computed accordingly,

$$L = \rho 4\pi R\frac{U_\infty^2}{\lambda}\sqrt{(1-a)^2 + (\lambda\mu(1+a'))^2}, \qquad \tan\phi = \frac{1-a}{\lambda\mu(1+a')}, \tag{3}$$

where U_∞ is the inflow velocity. For the drag mode, the additional drag forces are computed such that the total torque on the system is zero, ie

$$\int_{r_i}^{r_o} (L\sin(\phi)\times r)dr + \int_{r_i}^{r_o} (D\times r)dr = 0\,. \tag{4}$$

The number of on-board generators on the wing is set to two and the individual drag forces are each time divided over approximately 5% of the wing span, respectively at locations $\mu = 0.76$ and $\mu = 0.88$.

3. Results and discussion

3.1. Simulation setup

The numerical framework was verified against reference simulations presented in [8] for the turbine mode using full-span turbines blades instead of wings. In the present study, we perform simulations for both operation modes (turbine mode and drag mode) in laminar and turbulent inflows. The wing size and the path radius are chosen according to [1], in which an aircraft of type C-5A is following an orbital trajectory (at an angle of 0.4rad from the orbit axis) at a fixed tether length ($l_t = 400\,m$). The span length of the aircraft is $s = 68\,m$ and the path radius is $R = 155.77\,m$.The angular speed is set to represent a tip speed ratio $\lambda = 7$ at an inflow velocity $U_\infty = 10\,ms^{-1}$. The turbulent inflow is generated using the *tugen library* [17]. The parameters for the spectral tensor model are taken from [18] for turbulence over sea, assuming a wind velocity of $10ms^{-1}$ at a height $z = 180m$ which corresponds to the lower altitude bound at which airborne wind energy systems are meant to fly. The eddy length scale is $L_T = 60\,m$, the eddy dissipation scale is $\alpha\epsilon^{2/3} = 0.022\,m^{4/3}s^{-2}$, and the eddy lifetime parameter is $\Gamma = 2.85$.

The size of the computational domain is chosen such that the blockage ratio of the swept wing-area to the frontal domain area is small, ie. equal to 8%. The height and width of the domain are equal to 5.85 radii and the length is 23.42R. The last 10% of the domain length is used as fringe-region to impose the required inflow conditions. The rotation plane of the kite is situated 2.36 radii downstream from the domain inflow. The resolution of the numerical grid is $N_x \times N_y \times N_z = 640 \times 160 \times 320$ which corresponds to a grid cell size of approximately $5.70 \times 5.70 \times 2.85[m^3]$ that enables to capture the vortices shedding from the wing tips. A sketch of the computational domain is given in figure 1.

3.2. Wake characteristics

In this section we present wake characteristics of turbine and drag modes.

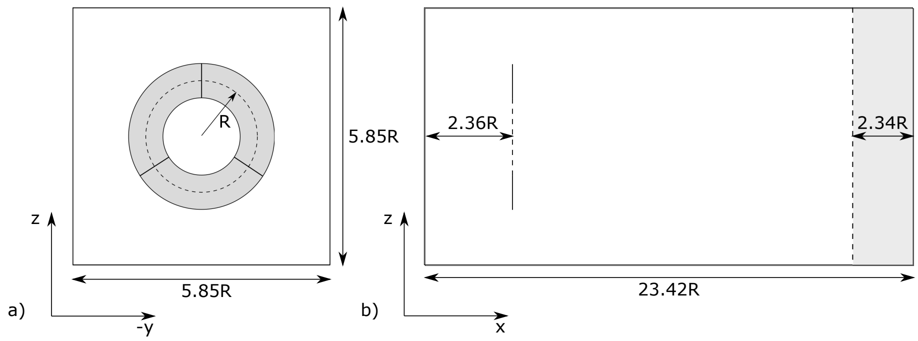

Figure 1. Computational domain used in this study; (a) cross-section; (b) side view.

The velocity induction in the wake is analysed by means of interference factors as shown in figure 2. The instantaneous axial interference factor is given by $a = 1 - U_x/U_\infty$, where U_x is the streamwise component of the velocity field. In figure 2.a, negative values of the axial induction factor indicate the location of tip vortices shedding from the wing in the annulus plane. Spreading of the wake is observable in positive and negative radial direction at downstream locations (fig.2.b-c). Due to the wake expansion, the surrounding flow as well as the flow in the core of the annulus is accelerated. In drag mode, no substantial difference in terms of axial induction is observed, thus induction of this mode is not shown here.

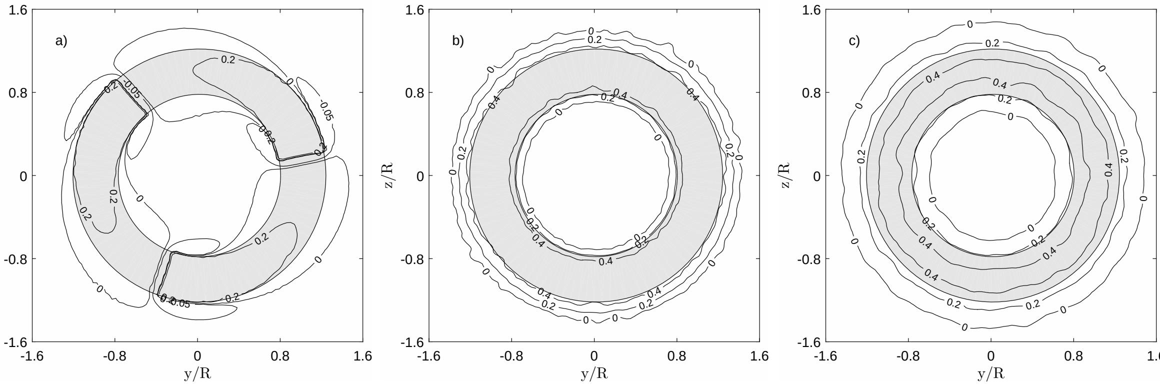

Figure 2. Axial induction factor of turbine mode for laminar inflow conditions; (a) Instantaneous distribution at annulus location; Time-averaged distribution downstream from annulus plane at (b) $x = 3R$ and (c) $x = 6R$.

The downstream wake development is shown in figure 3. In drag mode, we observe additional trailing vortices at the generator locations, associated to the modified lift force distribution. Although they rapidly break down between the annulus plane and $x/R \approx 1$, the wake mixing begins approximately at the same downstream location as in turbine mode, ie $x/R \approx 3$. The instantaneous location of the vortices with vorticity magnitude $|\omega| \geq 1.2s^{-1}$ is depicted in figure 4. In uniform inflow, the tip vortices are in both cases at the same position. From this we can see that the generator vortices have only little impact on the wake development. With turbulent inflow, the vorticity structure of the wake looses its coherence one radius downstream of the annulus plane, causing the wake to break down earlier. The additional perturbations due to drag mode do not seem to affect this process.

IOP Conf. Series: Journal of Physics: Conf. Series **854** (2017) 012019 doi:10.1088/1742-6596/854/1/012019

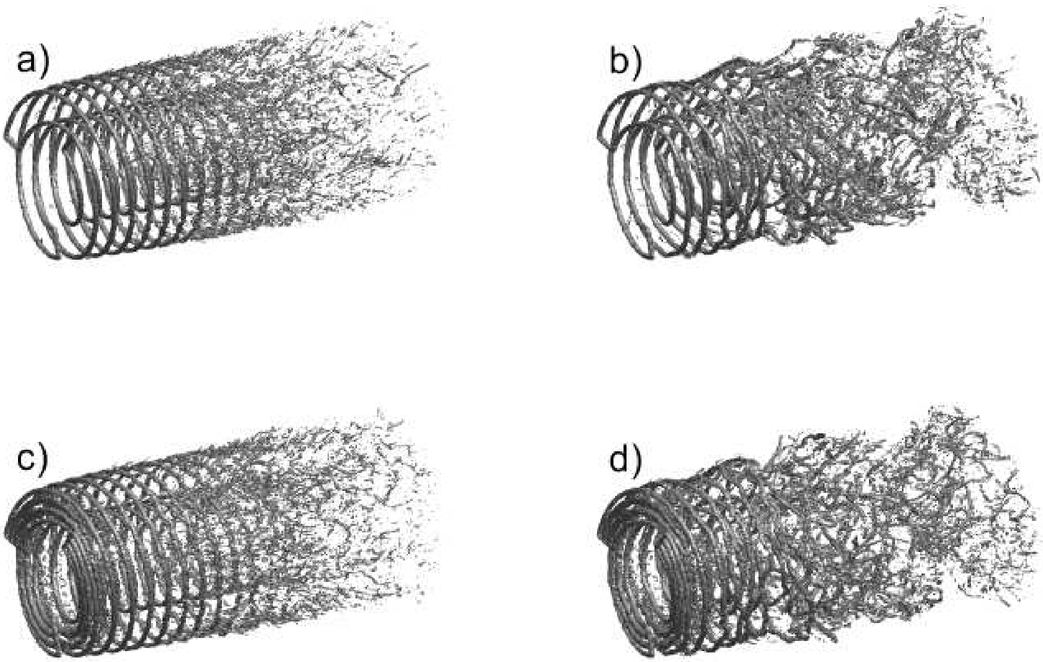

Figure 3. Downstream flow development visualized by vorticity isosurfaces; Turbine mode in (a) uniform and (b) turbulent inflow; Drag mode in (c) uniform and (d) turbulent inflow.

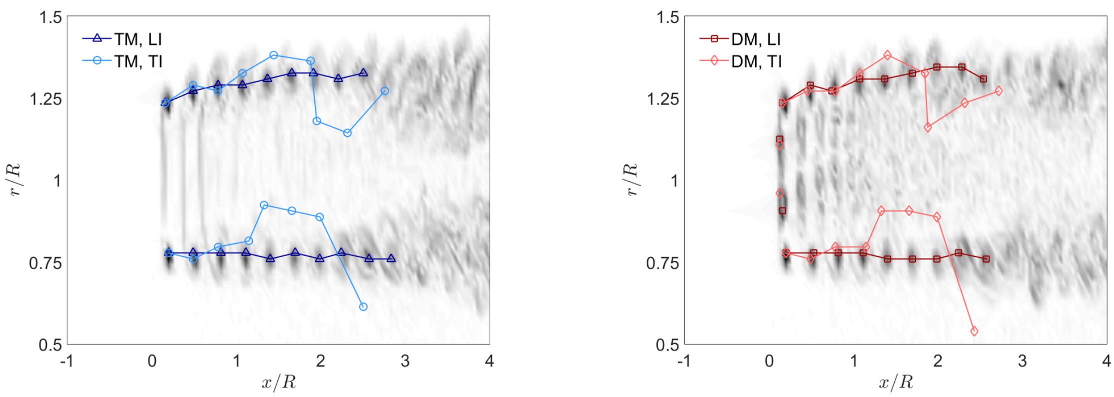

Figure 4. Instantaneous positions of vortices at $t = 360\,s$. (Left) Vorticity magnitude of turbine mode in laminar inflow is shown in background; instantaneous vortex positions in turbine mode for laminar (—△—) and turbulent (—○—) inflow. (Right) Vorticity magnitude of drag mode in laminar inflow is shown in background; instantaneous vortex positions in drag mode for laminar (—□—) and turbulent (—◇—) inflow.

Radial profiles of time-averaged axial velocity component are shown at the annulus plane, in the near wake ($x = 3R$, $x = 6R$) and in the far wake ($x = 9R$, $x = 12R$) in figure 5. Again, no difference is observable between turbine and drag modes. In turbulent inflow, the wake mixing increases and lead to a faster wake recovery in the far wake.

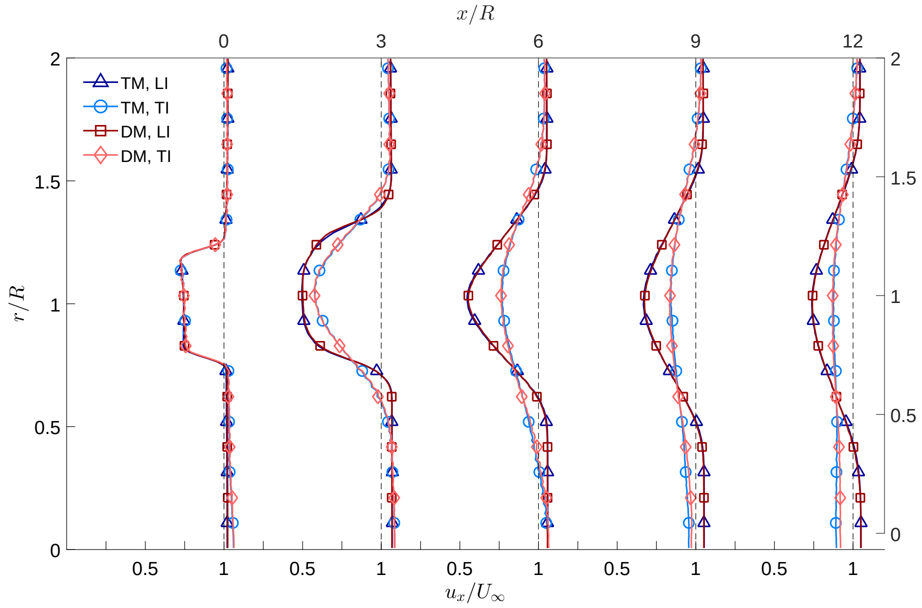

Figure 5. Radial profiles of time-averaged streamwise velocity component at different locations downstream of the annulus plane; Turbine mode in uniform (—▲—) and turbulent (—○—) inflows; Drag mode in uniform (—□—) and turbulent (—◇—) inflows.

4. Conclusions

In this paper, we have investigated the difference between two operation modes in the context of Airborne Wind Energy. Compared to a turbine-like mode, a torque-free operation mode of kite systems was presented. At the chosen operation and inflow conditions, this drag mode did not exhibit a different behaviour in terms of wake breakdown and recovery. The only feature specific to the drag mode was the shedding of additional vortices at the location of the on-board generators due to the modified force distribution along the wing. However, these vortices where not strong enough to interfere with the wing-tip vortices and had no substantial effect on the flow field. It is known from literature that the operation conditions of wind turbines, see for instance [9], affect the structure of the wake. Thus, simulations at different operation parameters (ie. tip-speed ratio) are required to further investigate the difference between the two modes introduced in this study. The addition of propellers onto the wing and the resulting modified near-rotor aerodynamics might also have an effect on the noise generation or the wind loading of the AWE system. These are interesting questions for further research. Next to that, an improved aerodynamic model also including the tether is of interest.

Acknowledgments

This project has received funding from the European Union's Horizon 2020 research and innovation programme under the Marie Skłodowska-Curie grant agreement No 642682. The computational resources and services used in this work were provided by the VSC (Flemish Supercomputer Center), funded by the Research Foundation Flanders (FWO) and the Flemish Government - department EWI.

References

[1] Loyd ML 1980 Crosswind kite power *J. Energy* **4** 106-11
[2] Diehl M 2013 Airborne Wind Energy: basic concepts and physical foundations *Airborne Wind Energy* ed U Ahrens *et al* (Berlin-Heidelberg: Springer) chapter 1 pp 3-22

[3] Fechner U 2016 Downscaling of airborne wind energy systems *J. Phys.: Conf Ser.* **753** 102002
[4] Coleman J, Ahmad H, Pican E and Toal D 2013 Non-reversing generators in a novel design for pumping mode airborne wind energy farm *Airborne Wind Energy* ed U Ahrens *et al* (Berlin-Heidelberg: Springer) chapter 34 pp 587-597
[5] Porté-Agel F, Wu Y T, Lu H and Conzemius R J 2011 Large-eddy simulation of atmospheric boundary layer flow through wind turbines and wind farms *J. Wind Eng. Ind. Aerodyn.* **99** 154-68
[6] Calaf M, Meneveau C and Meyers J 2010 Large eddy simulation study of fully developed wind-turbine array boundary layers *Phys. Fluids* **22** 015110
[7] Allaerts D and Meyers J 2017 Boundary-layer development and gravity waves in conventionally neutral wind farms *J. Fluid Mech.* **814** 95-130
[8] Sørensen J N and Shen W Z 2002 Numerical modeling of wind turbine wakes *J. Fluids Eng.* **124** 393-99
[9] Troldborg N, Sørensen J N and Mikkelsen R 2010 Numerical simulations of wake characteristics of a wind turbine in uniform inflow *Wind Energ.* **13** 86-99
[10] Iungo G V, Viola F, Camarri S, Porté-Agel F and Gallaire F 2013 Linear stability analysis of wind turbine wakes performed on wind tunnel measurements *J. Fluid Mech.* **737** 499-526
[11] Sørensen J N 2011 Instability of helical tip vortices in rotor wakes *J. Fluid Mech.* **682** 1-4
[12] Cherubini A, Papini A, Vertechy R and Fontana M 2015 Airborne wind energy systems: a review of the technologies *Renew. Sustainable Energy Rev.* **51** 1461-76
[13] Burton T, Jenkins N, Sharpe D and Bossanyi E 2011 *Wind Energy Handbook* John Wiley & Sons Ltd
[14] Goit J and Meyers J 2015 Optimal control of energy extraction in wind-farm boundary layers *J. Fluid Mech.***768** 5-50
[15] Munters W, Meneveau C and Meyers J 2016 Turbulent inflow precursor method with time-varying directions for large-eddy simulations and applications to wind farms *Boundary-Layer Meteorol.***159** 305-28
[16] Nordström J, Nordin N and Henningson D 1999 The fringe region technique and the fourier method used in direct numerical simulation of spatially evolving viscous flows *SIAM J. Sci. Comput.***20** 1365-93
[17] Gilling L 2009 Tugen - synthetic turbulence generator manual and user's guide. Technical report. Aalborg University. Aalborg
[18] Mann J 1998 Wind field simulation *Prob. Engng. Mech.* **13** 269-82